# Single-Cell Multi-omics Decodes the Aggrephagy Landscape, Unveiling TUBA4A as a Novel Oncogene and Immunotherapeutic Target in ccRCC

Kun Cui[1*], Qiuxin Duan[1*], Zhe Xu[1,2*], Wenjing Liu[1*], Yueli Ni[1], Yongping Li[1], Lu Yuan[1], Zhuoran Teng[1], Yurong Dong[3], Ziyuan Bai[3], Asif Shahzad[1], Jinshan Zhang[1], Yu Dou[1], Jiaojiao Xia[1], Hanyue Shao[1], Zhe Yang[3], Qiao Zhang[1]

[1]Department of Biochemistry and Molecular Biology, School of Basic Medical Sciences, Kunming Medical University, Yunnan, Kunming 650500, P.R. China

[2] Qujing Medical College, Yunnan, Qujing 655011, P.R. China

[3]Departments of Pathology, The First Affiliated Hospital of Kunming Medical University, Yunnan, Kunming 650032, P.R. China

[*]Contributed equally

*Correspondence to*:

Professor Qiao Zhang, Department of Biochemistry and Molecular Biology, School of Basic Medical Sciences, Kunming Medical University, 1168 Yuhua Road, Chenggong, Yunnan, Kunming 650500, P.R. China. E-mail: zhangqiao200824@126.com

Professor Zhe Yang, Department of Pathology, The First Affiliated Hospital of Kunming Medical University, 295 Xichang Road, Wuhua, Yunnan, Kunming 650032, P.R. China. E-mail: yangzhe@ydyy.cn

## Associated Data

### Supplementary Materials

**Additional files Figure S3, S5 and S6.** The prognosis of novel aggrephagy cell clusters was evaluated in the TCGA cohort, RECA-EU cohort, and E-MTAB-1980 cohort.

The immune response of patients with ccRCC was evaluated by novel aggrephagy cell clusters in the TCGA cohort.

**Additional file 2 Figure S4.** The prognosis and immune response of patients with ccRCC were evaluated by novel aggrephagy cell clusters in the IMvigor210 cohort.

### Data Availability Statement

All data generated or analyzed during this study are included in this published article.

### Abstract

Clear cell renal cell carcinoma (ccRCC) is an aggressive malignancy with a complex and immunosuppressive tumor microenvironment (TME). While aggrephagy, a selective autophagy process, has been linked to cancer, its role in ccRCC remains unclear. Through integrated multi-omics analysis of single-cell and bulk sequencing

data, we constructed the first aggrephagy activity atlas in ccRCC TME, revealing subtype-specific programs linked to immune suppression and metabolic reprogramming. High aggrephagy activity correlated with poor prognosis and immunotherapy resistance, particularly in macrophages and T cells. Among key prognostic genes, we identified TUBA4A as a novel player in ccRCC. Functional validation showed that TUBA4A enhances autophagy and promotes tumor proliferation, migration, and invasion. This study establishes aggrephagy and TUBA4A as key regulators of ccRCC progression and potential therapeutic targets.

**Keywords:** ccRCC, aggrephagy, tumor microenvironment, prognosis

## 1. Introduction

Renal cell carcinoma (RCC) ranks within the top 10 most prevalent cancers globally, contributing to 2–5 percent of all malignancies, particularly notable in developed countries [1, 2]. As the most lethal urologic cancer, it is responsible for over 10,000 deaths annually and has a 5-year survival rate of around 75% [3, 4]. Despite advances in targeted therapies like VEGF inhibitors, TKIs, and mTOR inhibitors [5-7], the overall outcomes for high-risk patients, especially those with aggressive clear cell renal cell carcinoma (ccRCC), the most common subtype of RCC, remain unsatisfactory [8, 9]. The main reasons for the poor outcomes are the high incidence of ccRCC, late diagnosis, tendency to metastasize, and significant chemotherapy resistance [10]. Moreover, tumor heterogeneity, reflected in diverse tumor microenvironment (TME) compositions and cancer cell populations, plays a central role in treatment failure and drug resistance [11].

The TME constitutes a highly organized and interactive network comprising malignant cells, immune populations, inflammatory mediators, and stromal components such as cancer-associated fibroblasts. Tumors actively engineer the TME by inducing angiogenic programs, establishing metabolic co-dependencies with stromal elements, and evading immune surveillance through localized immunosuppression [12-14]. In turn, the cellular and non-cellular constituents of the TME exert profound influences on tumor growth, differentiation, and clonal evolution. A major obstacle in

TME research stems from extensive intra- and intertumoral heterogeneity, which conventional bulk sequencing fails to resolve, as it averages gene expression across diverse cell types and states [15]. Single-cell RNA sequencing (scRNA-Seq) offers a transformative solution by enabling quantitative transcriptome-wide profiling at individual cell resolution, thus uncovering the functional diversity, developmental trajectories, and cell-cell signaling events that collectively shape the TME [16, 17].

Autophagy is an evolutionarily conserved process that degrades cytoplasmic components such as organelles and proteins to maintain cellular homeostasis [18]. It provides a critical source of biomolecules and energy under stress conditions, including those within the TME [19]. The accumulation of misfolded protein aggregates, which is often exacerbated by TME-associated stresses such as hypoxia, nutrient deprivation, and proteotoxic stress, disrupts normal cellular functions [20, 21]. Aggrephagy, a selective form of autophagy, specifically targets these harmful aggregates for degradation and serves as a key quality control mechanism. Its dysfunction has been linked to neurodegenerative diseases, cancer, and metabolic disorders [22]. Within the TME, impaired aggrephagy can promote tumor progression by allowing the persistence of aggregated proteins that disrupt key tumor suppressors such as p53. Notably, protein misfolding and aggregation can impair p53 function, leading to loss of tumor suppressor activity and promoting cancer progression [23-25]. Therefore, aggrephagy represents an adaptive response to proteotoxic stress in the TME, and understanding its role may open new avenues for targeted cancer therapies.

The TME of ccRCC plays a critical role in disease progression, yet the function of aggrephagy, a selective autophagic process, within this context remains unexplored. To address this gap, we constructed a comprehensive single-cell atlas of ccRCC TME cell types (stromal, myeloid, lymphoid, and fibroblasts), revealing widespread aggrephagy-related mRNA expression patterns linked to intercellular communication and tumor suppression. NMF analysis of 44 aggrephagy-associated genes [26] uncovered subtype-specific expression modules correlated with endothelial interaction, immune activity, metabolic reprogramming, and transcriptional regulation. Integration with bulk RNA-seq data further established aggrephagy-defined cellular clusters as predictors of patient

survival and immunotherapy response. Critically, multi-cohort analysis identified four consistently prognostic genes, among which TUBA4A, a previously uncharacterized α-tubulin isotype in ccRCC, exhibited strong clinical relevance [27]. TUBA4A is known to exhibit tissue-specific expression and mutation-associated pathogenicity, underscoring its functional specificity. This study provides the first evidence implicating TUBA4A and aggrephagy in ccRCC TME regulation, highlighting their potential as prognostic biomarkers and therapeutic targets.

## 2. Materials and Methods

### 2.1 Data collection

We conducted an extensive analysis by gathering data from multiple sources. Our investigation involved single-cell transcriptome sequencing data from specific samples, including two ccRCC samples (GSM4630028 and GSM4630029) and one normal kidney sample (GSM4630031) from the GSE152938 dataset [28]. Additionally, we examined seven ccRCC tissues and two adjacent tissues from the GSE210038 dataset [29]. We focused on primary tumors and non-tumor ccRCC tissue for in-depth analysis. For a broader perspective, we obtained transcriptomic data and clinical prognosis-related information from The Cancer Genome Atlas (TCGA), comprising 537 ccRCC samples and 72 adjacent normal tissue samples. To validate our findings, we incorporated transcriptomic data from 91 samples in the International Cancer Genome Consortium (ICGC) renal cell cancer cohort (RECA-EU) and data from 101 samples in the E-MTAB-1980 cohort from the EMBL-EBI database. Furthermore, we utilized data from the IMvigor210 dataset [30], which includes information on individuals treated with PD-(L)1 along with their clinical characteristics. In addition to these datasets, we gathered a list of 44 genes related to aggrephagy from the MSigDB database [31] for further analysis.

### 2.2 scRNA-seq data process

To visualize the TME cell types present in ccRCC, we utilized the R package “Seurat” to generate Seurat objects and systematically carried out the processes of normalization, integration, dimension reduction, and clustering using the Seurat pipeline [32]. A comprehensive set of 39,423 genes and 86,847 cells underwent

thorough quality control (QC) procedures (Figure S1A). Cells deemed as low-quality were filtered out by excluding those with fewer than 200 unique molecular identifiers (UMIs) and those exhibiting gene expression levels either surpassing 4,500 or falling below 200 cells. Moreover, cells classified as dead or dying were identified and removed based on having more than 15% UMIs originating from the mitochondrial genome (Figure S1B). Consequently, a total of 75,144 high-quality cells were successfully obtained across all sample sets. These cells were uniformly distributed within the ccRCC samples, with gene expression levels demonstrating a strong positive correlation with the extent of gene expression (0.93) (Figure 1A). To establish dimensionality reduction, a scale matrix containing 3,000 highly variable genes was meticulously chosen (Figure 1B). The highly variable genes underwent normalization via PCA and were visually depicted using DimPlot and ElbowPlot (Figure 1C). To integrate tissue and patient samples, the R package "harmony" was proficiently utilized for data scaling and integration purposes (Figure 1D). UMAP was employed for data visualization, while cell annotation was expertly conducted by published literature [33, 34], referencing common tumor microenvironment cell markers and the CellMarker website [35]. Figures 1E and S1D illustrate the overall design of the study.

**2.3 Non-negative matrix factorization of aggrephagy genes in TME cells**

To explore the role of 44 aggrephagy genes in various TME cell types, an expression matrix comprising these genes was developed. Cells lacking expression of any aggrephagy genes were excluded from the analysis. Utilizing the "NMF (non-negative matrix factorization)" package, matrix decomposition was conducted, subsequently followed by clustering for dimensionality reduction. The methodology used in this study has been documented in relevant literature [36, 37].

**2.4 Identification of cellular subtype marker genes associated with aggrephagy genes in TME cells**

We further classified NMF cell subsets by reannotating them according to specific criteria, which involved identifying characteristic genes for each cluster. Annotation was conducted based on the following criteria: 1) logFC > 1, where the top-ranked signature gene was an aggrephagy gene; 2) logFC > 1 without expression of aggrephagy

genes, indicating genes unrelated to aggrephagy; 3) logFC < 1 with an unclear association with aggrephagy genes.

### 2.5 Pseudo-temporal trajectory analysis of aggrephagy genes in TME cells

Our study focused on exploring the single-cell trajectory analysis involving aggrephagy in the ccRCC TME through the application of the “Monocle” R package [38]. For this analysis, we conducted developmental sorting of all subtypes of cells in ccRCC, with specific criteria set at mean_expression >= 0.1 and dispersion_empirical >= 1 * dispersion_fit. Data downscaling was achieved using the 'DDRTree' method. The visualization of aggrephagy distribution was integrated into the developmental trajectory of different TME cell clusters identified by NMF.

### 2.6 Cell communication analysis for NMF aggrephagy-related subtypes of cells

To explore cellular interactions between NMF aggrephagy cell types, we performed intercellular ligand-receptor analysis using CellChat, an R package that identifies and quantifies intercellular communication within single-cell datasets [39]. Initially, we isolated NMF aggrephagy cell subtypes and immune cells, followed by the identification of overexpressed genes and ligand-receptor pairs. Subsequently, we projected the ligands and receptors to the Protein-Protein Interaction (PPI) network for weight analysis. Additionally, secreted signaling in ccRCC was included in the cell-cell interaction analysis [40].

### 2.7 SCENIC analysis for aggrephagy-related subtypes

We utilized the “pySCENIC” package [41], a Python-based implementation of the SCENIC pipeline, to investigate the transcription factor (TF) gene regulatory network in ccRCC. Our study started by removing genes that were expressed in less than 1% of cells and only kept those that were present in the RcisTarget database. Subsequently, we utilized the “runCorrelation” function to create a correlation matrix of the genes and pinpointed potential targets for each transcription factor through GENIE3. Following that, we conducted a regression analysis on the correlation between TFs and targets. To handle the numerous cell types, we utilized the Regulon Specificity Score (RSS) to pinpoint regulons specific to each cell type and created a heatmap of regulon scores.

We further improved visualization using the "ComplexHeatmap", "ggplot2", and "pheatmap" packages.

**2.8 Functional enrichment analysis of NMF aggrephagy-related subtypes**

To investigate the metabolic properties of aggrephagy-related subtypes identified using NMF typing, an enrichment score analysis was performed. For demonstration purposes, the "scmetabolism" package [42] was utilized to randomly generate scores for 30 metabolic signaling pathways.

**2.9 Prognostic analysis and Immunotherapeutic response of NMF aggrephagy-related subtype cells**

We examined the prognostic and immune response implications of NMF aggrephagy subtypes in various ccRCC cohorts, including TCGA-KIRC, RECA-EU, and E-MTAB-1980, at the bulk level. The gene signature scores for the aggrephagy cell subtypes were calculated using the "GSVA" package [43]. The association between NMF signatures related to aggrephagy and patient prognosis was investigated through optimal Cutoff, log-rank test, and Cox proportional hazard regression analysis. Kaplan-Meier curves were generated, and cutoff values for different NMF cell signatures in diverse ccRCC cohorts were determined using the "survminer" package. The immunotherapeutic responses of NMF aggrephagy-related subtypes were predicted using the TIDE database [44], which evaluates patient response based on expression profiles before tumor treatment, utilizing various established transcriptional biomarkers.

**2.10 Cell culture, treatment and transfection**

ACHN (CRL-1611; ATCC), 786-O (CRL-1932; ATCC), Caki-1 (HTB-46; ATCC) were sourced from the Kunming Institute of Zoology, Chinese Academy of Sciences. The 293T cell line (CRL-3216TM; ATCC) was obtained from Land. Hua Gene Biosciences. All cell lines were maintained under standard culture conditions as previously described [45]. For functional assays, ACHN and Caki-1 cells were transfected with a TUBA4A overexpression plasmid or a corresponding control plasmid. Plasmids and vectors were supplied by GeneCreate Biological Engineering Co., Ltd. (Wuhan, China). Transfection was performed using 2.5 μl Lipofectamine 2000 reagent (11668500, Thermo Fisher Scientific, Waltham, MA, USA) following the

manufacturer's instructions. After 6–8 h, the medium was replaced with fresh medium containing 10% FBS, and cells were further incubated for 24 h. Transfected cells were then harvested for protein extraction, and TUBA4A expression was confirmed by Western blotting. Successfully transfected cells were subsequently used for downstream experiments.

**2.11 Protein analysis of prognostic genes**

The UALCAN platform, which integrates TCGA RNA-seq, clinical, and prognostic data for 31 cancer types [46], was used to assess the expression of four prognostic proteins in ccRCC (n = 219) versus normal tissues (n = 169) based on CPTAC datasets [46, 47]. Proteomic analysis of 20 paired ccRCC and adjacent normal tissues, collected post-surgery and snap-frozen at –80 °C, was performed using a Thermo Fisher Q Exactive mass spectrometer at Shanghai Applied Protein Technology Co., Ltd. Proteins with fold changes >2.0 or <0.5 and $p < 0.05$ were considered significant. To further validate TUBA4A expression, immunohistochemistry (IHC) data were retrieved from the Human Protein Atlas (HPA) [48].

For Western blot assays, cells were lysed in RIPA buffer (R0020, Solarbio, Beijing) supplemented with protease/phosphatase inhibitors (P0100, Solarbio). Protein concentrations were determined with a BCA kit (P1511, Applygen, Beijing). Equal protein amounts (40 μg/sample) were separated by 10% SDS-PAGE, transferred to PVDF membranes (IPVH00010, Millipore), and incubated overnight at 4 °C with primary antibodies, followed by secondary antibody incubation (1 h, RT). Protein bands were visualized using an ECL kit (K-12045-D50, Bioship) on a Bio-Rad ChemiDoc XRS system. Antibodies used included anti-TUBA4A (#D110022, Sangon), anti-LC3 (#14600-1-AP, Proteintech), and anti-P62 (#18420-1-AP, Proteintech); fluorescent secondary antibody: anti-rabbit IgG (#ab6721, Abcam). All experiments were performed in triplicate.

**2.12 MTS assay, Wound healing assay, Transwell migration assay and Transwell invasion assay**

ccRCC cells ($2.5\times10^3$/well) and controls were seeded in 96-well plates. Cell viability was assessed at 0, 24, 48, 72, and 96 h by adding 20 μl MTS reagent (CTB169,

Promega, WI, USA) per well, incubating for 1 h at 37 °C, and measuring absorbance at 490 nm with a microplate reader (51119200, Thermo Fisher Scientific, Waltham, MA, USA). Relative proliferation rates were calculated according to the manufacturer's instructions. For wound-healing assays, cells were seeded in six-well plates, allowed to adhere overnight, and scratched with a 20 µl pipette tip. Images were captured at 0 and 24 h by fluorescence microscopy, and wound closure was quantified using ImageJ software. For invasion assays, Transwell chambers (3524, Corning, USA) pre-coated with Matrigel (1:8 dilution, 356234, BD Biosciences, NJ, USA) were seeded with cells suspended in serum-free medium in the upper chamber, while the lower chamber contained DMEM supplemented with 10% FBS. After 24 h, invaded cells were fixed with 4% paraformaldehyde, stained with crystal violet, and imaged by fluorescence microscopy.

### 2.13 Statistical analysis

To analyze discrepancies among subgroups of various subtypes, we utilized the Student's t-test, Wilcoxon rank-sum, and Kruskal-Wallis tests. We identified genes associated with TME and various types of CAFs, tumor-associated macrophages (TAMs), CD8+ T cells, and B cells for correlational assessment concerning subtype cells. R 4.1.2 software was used for all statistical evaluations, with p-values less than 0.05 deemed as statistically significant. In addition, to evaluate the prognostic value of TUBA4A, we performed Kaplan–Meier analysis with log-rank testing (survminer v0.4.9). ccRCC patients were stratified into low- and high-TUBA4A expression groups. Univariate Cox regression was used to estimate hazard ratios (HR) and 95% confidence intervals (CI). Significant variables ($p < 0.1$) from univariate analysis were included in a multivariate Cox model for further mortality risk assessment.

## 3. Results

### 3.1 An overview of aggrephagy-related genes in single-cell data from ccRCC is provided.

We investigated genes associated with aggrephagy within the ccRCC landscape by analyzing single-cell data from nine ccRCC tissues and three normal kidney tissues, in

addition to three ccRCC prognosis datasets and an immunotherapy dataset. The annotation of cells was carried out using marker genes sourced from existing literature, with a focus on NK cells, T cells, epithelial cells, endothelial cells, fibroblasts, macrophages, monocytes, mast cells, and B cells (Figures 2A and 2B). Notable differences in the composition of cell types were observed between tumor and normal tissues, with particular emphasis on epithelial cells, endothelial cells, fibroblasts, and T cells (Figure 2C). Analysis through CellChat revealed the interactions among different subtypes of cells (Figures 2D and 2E), as well as the intensity of these interactions through ligand-receptor pairs (Figure 2F). A heat map was used to illustrate the expression of 44 aggrephagy-related genes across various TME cell types, providing insights into their differential expression patterns (Figure 2G). Violin plots emphasized the high expression levels of DYNLL1, HSP90AA1, RPS27A, TUBB4B, UBA52, UBB, UBC, and VIM genes across multiple cell types (Figure 2H). These results suggest that the expression of aggrephagy genes could influence intercellular communications within the tumor microenvironment.

### 3.2 Novel fibroblast clusters are evaluated under aggrephagy gene modifications

Recent studies have identified CAFs as a crucial element in the TME and are becoming a focal point of research [49]. We conducted a dimension reduction analysis to explore the impact of aggrephagy expression on CAFs. Through pseudo-temporal analysis, we identified six clusters of genes related to aggrephagy that play important roles in various stages of CAF development (Figure 3A). During the early stages of CAF development, genes such as UBE2N, DYNC1LI2, and PARK7 showed significant expression, while PCNT, TUBA1C, and TUBA4A were prominent in later stages. By using NMF, we categorized CAF subtype cells based on the expression of aggrephagy-related genes into Unclear-CAF-C0, DYNC1I2+CAF-C1, TUBB4B+CAF-C2, and Non-aggrephagy-CAF-C3 subtypes (Figures 3B and 3C). The developmental trajectory of NMF-based CAF clusters varied significantly based on pseudotime analysis (Figure 3D). Fibroblasts play a crucial role in the tumor stroma. CAFs and the acidic microenvironment promote tumor cells to favor glucose metabolism and enhance tumor progression [50]. Therefore, identifying different aggrephagy cells can help in

understanding the relationships and coordination among aggrephagy fibroblasts. Endothelial cells were mainly associated with DYNC1I2+CAF-C1 cell clusters (Figures 3E and 3F). Moreover, DYNC1I2+CAF-C1 cell clusters exhibited the highest levels of Outgoing and Incoming signaling patterns (Figure 3G), with PDGF, PTN, and GAS being the key signaling pathways involved in tumor proliferation and migration. We also examined important CAF phenotype markers, such as pro-inflammatory genes, neo-angiogenic genes, and MMPs. The pathway heatmap (Figure 3H) displayed distinct expression patterns of common pathway genes among aggrephagy-CAF subtypes. DYNC1I2+CAF-C1 exhibited significantly elevated expression levels of ECM, TGFb, Neo-Angio, and proinflammatory pathway genes, while TUBB4B+CAF-C2 displayed significantly higher expression of ECM, Neo-Angio, Contractile, and Ras pathway genes. We performed a comparative analysis of TF regulation characteristics and subtype-specific transcription factors between DYNC1I2+CAF-C1 and TUBB4B+CAF-C2. Our findings indicated that, except for a few transcription factors, the expression patterns of other transcription factors demonstrated an inverse trend (Figure 3I). Additionally, DYNC1I2+CAF-C1 and Unclear-CAF-C0 cell clusters were identified as being more enriched in metabolic signaling pathways (Figure S2A). NMF cluster 2 (TUBB4B+CAF-C2) showed enrichment in the signaling pathway associated with protein processing in the endoplasmic reticulum (Figure 3J). GSVA was utilized to calculate scores for established classical CAF phenotype markers, intending to reveal the potential phenotypes and functionalities of the aggrephagy CAF subtypes [51]. DYNC1I2+CAF-C1 demonstrated the highest scores for pan-myCAF, pan-dCAF, and pan-pCAF, whereas TUBB4B+CAF-C2 exhibited prominent scores for pan-iCAF and pan-iCAF-2 (Figure 3K). Consequently, our identified fibroblast clusters associated with aggrephagy can be related, to some degree, to classical fiber phenotypes [52].

### 3.3 Novel macrophage cell clusters are studied under aggrephagy gene modifications

In ccRCC tissue, TAMs are present and play a critical role in the advancement and prognosis of the disease. A thorough analysis of gene expression patterns in macrophage development revealed diverse expressions of aggrephagy genes at different stages,

indicating their intricate functions in regulating macrophage differentiation and activity (Figure 4A). Through NMF clustering and gene annotation, novel macrophage subpopulations were identified, including TUBB4B+Mac-C0, Non-aggrephagy-Mac-C1, TUBA1A+Mac-C2, HSP90AA1+Mac-C3, and DYNC1H1+Mac-C4 (Figure 4B). Notably, TUBB4B+Mac-C0 comprised the largest portion of macrophages (Figure 4C), with varying degrees of development observed across TAM clusters in the pseudotime analysis (Figure 4D). The visualization of interactions between different macrophage subpopulations using CellChat revealed that TUBB4B+Mac-C0 had the highest interaction with endothelial cells at 7 (Figures 4E and 4F). Furthermore, TUBB4B+Mac-C0, TUBA1A+Mac-C2, HSP90AA1+Mac-C3, and DYNC1H1+Mac-C4 were associated with numerous outgoing and incoming signaling pathways, with key factors such as MIF, COMPLEMENT, GALECTIN, SPP1, ANNEXIN, TNF, and TGFb contributing significantly to these interactions (Figure 4G). The transcriptional activity was notably high in the HSP90AA1+Mac-C3 cluster (Figure 4H). NMF cluster 1 (Non-aggrephagy-Mac-C1) showed enrichment in rheumatoid arthritis, lipid and atherosclerosis, and Chagas disease, while NMF cluster 3 (HSP90AA1+Mac-C3) exhibited enrichment in protein processing in the endoplasmic reticulum (Figure 4I). Additionally, TUBA1A+Mac-C2 was enriched in various metabolism-related signaling pathways (Figure S2B). Subsequently, we conducted a comparison of newly identified aggrephagy-associated macrophage subpopulations with respect to M1 and M2 macrophage classifications. Additionally, the polarization scores indicative of M1-like and M2-like characteristics were calculated for various aggrephagy TAM subtypes, as referenced in [53]. As shown in Figures 4J and S1D, the novel aggrephagy macrophage cell clusters are mainly concentrated with the M1-type cell subpopulation. TAMs in ccRCC play a critical role in tumor progression by promoting proliferation, angiogenesis, immune escape, and dissemination, and their dual M1/M2 properties make them a promising therapeutic target requiring further investigation for specific markers [54].

### 3.4 Novel $CD8^+$ T cell clusters are analyzed under aggrephagy gene modifications

The researchers further classified the T cells into subpopulations identified as $CD4^+$ T, $CD8^+$ T, and NK cells. Given the critical role of $CD8^+$ T cells in affecting tumor metastasis and treatment outcomes, an in-depth analysis of these cells was undertaken [55]. Using Monocle2, it was observed that the expression patterns of aggrephagy genes varied across different stages of macrophage development, suggesting their intricate and dynamic roles in the differentiation and functional regulation of macrophages (Figure 5A). $CD8^+$ T cells were subdivided into six clusters via NMF, annotated with aggrephagy genes: Unclear-$CD8^+$T_cells-C0, $TUBA1A^+$CD8+T_cells-C1, TUBA1B+$CD8^+$T_cells-C2, TUBA4A+ $CD8^+$T_cells-C3, TUBB4B+$CD8^+$T_cells-C4, and Non-aggrephagy-$CD8^+$T_cells-C5 (Figure 5B). The expression of aggrephagy genes within $CD8^+$ T cell clusters varied across nine ccRCC patients (Figure 5C). The novel $CD8^+$ T cell cluster was further categorized into four branches according to a proposed temporal sequence (Figure 5D). Concurrently, CellChat analysis demonstrated the strength of the correlation among the novel aggrephagy $CD8^+$ T cell clusters. By examining the interactions between various novel aggrephagy $CD8^+$ T cells and endothelial cells, it was found that TUBA1B+$CD8^+$T_cells-C2 had the highest number of interactions (Figure 5E). CellChat signaling analysis indicated that the main incoming signaling routes for aggrephagy $CD8^+$ T cell clusters were through the PARs, CD137, and VISFATIN signaling pathways. The MIF and CD137 signaling pathways emerged as the primary outgoing signaling routes for the novel aggrephagy $CD8^+$ T subtype (Figure 5F). Additionally, the interaction between immune checkpoints and their corresponding ligands (such as PD-1/PD-L1 and CTLA4/CD86) plays a role in altering the metabolism of both tumor and immune cells [56]. A study was conducted to compare the average expression levels of genes associated with immune checkpoint activators and suppressors in various subsets of $CD8^+$ T cells. As a result, six distinct clusters of aggrephagy $CD8^+$ T cells displayed varying immune function-related terms (Figures 5G and 5H). Transcription factors are capable of modulating the expression of genes downstream and act as key regulators in maintaining cellular characteristics. It was observed that the TUBA1B+$CD8^+$T_cells-C2 and Non-aggrephagy-$CD8^+$T_cells-C5 clusters exhibited heightened transcription factor activity (Figure 5I). The

TUBA1B+CD8$^+$T_cells-C2 cell clusters were notably enriched in a variety of metabolic signaling pathways (Figure S2C). Most cell clusters demonstrated enrichment in Parkinson's disease, whereas NMF cluster 2 (TUBA1B+CD8$^+$T_cells-C2) was specifically enriched in the cell cycle pathway (Figure 5J). Interestingly, the analysis revealed that TUBA1A+CD8$^+$T_cells-C1 and TUBA1B+CD8$^+$T_cells-C2 displayed elevated T cytotoxic and T exhaustion scores, whereas TUBA4A+CD8$^+$T_cells-C3 and TUBB4B+CD8$^+$T_cells-C4 exhibited lower scores for both metrics (Figure 5K).

### 3.5 Novel B cell clusters are investigated under aggrephagy gene modifications

As integral components of the immune system, B cells are crucial for antibody production, immune regulation, and memory response. By utilizing genes associated with aggrephagy, B cells were further categorized into four groups: TUBA1A+B_cells-C0, UBC+B_cells-C1, Non-aggrephagy-B_cells-C2, and DYNC1H1+B_cells-C3 (Figure 6A). Among these, TUBA1A+B_cells-C0 cell clusters constituted 28%, UBC+B_cells-C1 cell clusters comprised 23%, and DYNC1H1+B_cells-C3 cell clusters made up 18% of the total B cell population (Figures 6B, 6C and 6D). Results from CellChat analysis demonstrated that these novel B cell subtypes interacted with endothelial cells across the four distinct aggrephagy B cell clusters (Figures 6E and 6F). The MIF signal was found to be the predominant contributor to both the output and input signals within these cell clusters (Figure 6G). Additionally, higher transcription factor activity was found in UBC+B_cells-C1 clusters (Figure 6H). Numerous metabolic pathways were found to be enriched in UBC+B_cells-C1 cell clusters (Figure S2D). Furthermore, the NMF cell cluster 1 (UBC+B_cells-C1) showed significant enrichment in protein processing activities within the endoplasmic reticulum (Figure 6H).

### 3.6 The prognosis and immune response of patients with ccRCC are influenced by novel aggrephagy cell clusters

Further, we analyzed the prognosis of the subtype cells using transcriptional and prognostic information from the TCGA, RECA-EU, and E-MATB-1980 cohorts. According to CellChat, all aggrephagy cell subtypes in ccRCC interact with one another

(Figure 7A). Specifically, TUBB4B+Mac-C0 and DYNC1H1+Mac-C4 cell clusters showed more frequent interactions with endothelial cells (Figure 7B). A box plot illustrates that aggrephagy-related genes exhibit lower expression in tumor tissues compared to normal tissues within the TCGA-KIRC cohort (Figure 7C). Moreover, our findings indicate that cell types like DYNC1I2+CAF-C1, TUBB4B+CAF-C2, and TUBA1A+CD8$^+$T_cells-C1 are significantly less expressed in tumor tissues compared to normal tissues ($p < 0.05$) (Figure 7D). On the other hand, cell types such as TUBA1B+CD8$^+$T_cells-C2, TUBA4A+CD8$^+$T_cells-C3, TUBB4B+CD8$^+$T_cells-C4, TUBA1A+Mac-C2, HSP90AA1+Mac-C3, DYNC1H1+Mac-C4, TUBA1A+B_cells-C0, UBC+B_cells-C1, and DYNC1H1+B_cells_C3 are significantly overexpressed in tumor tissues relative to normal tissues ($p < 0.05$) (Figure 7D). Subsequent univariate Cox analysis provided consistent prognostic information for novel aggrephagy subtypes across different datasets (Figure 7E). Cell clusters such as TUBA1A+CD8$^+$T_cells-C1 and TUBA1B+CD8$^+$T_cells-C2 could serve as potential risk factors for patients with ccRCC. After confirming the influence of aggrephagy on the TME, we assessed whether these aggrephagy-based TME patterns influenced responses to ICB therapy. Moreover, the prognosis of these novel aggrephagy cell clusters was examined in different datasets available in the immunotherapy TIDE database. The TCGA, RECA-EU, and E-MATB-1980 cohorts revealed varying immunotherapeutic responses for multiple aggrephagy cell subtypes ($p < 0.05$) (Figures 7G, 7H, and 7I). Furthermore, our analysis revealed that within at least two cohorts, TUBB4B+CAF-C2, TUBA1B+CD8$^+$T_cells-C2, TUBA4A+CD8$^+$T_cells-C3, TUBB4B+CD8$^+$T_cells-C4, TUBB4B+Mac-C0, UBC+B_cells-C1, and DYNC1H1+B_cells_C3 were found to be downregulated in responders, indicating a potential association with resistance to immune checkpoint blockade (ICB) (Figures 7G-7I). By employing logistic regression, we calculated the odds ratio for predicting response, highlighting the negative impact of these specific cell types (Figure 7F). The IMvigor210 cohort comprised patients with advanced uroepithelial carcinoma who received anti-PDL1 therapy. In this cohort, DYNC1I2+CAF-C1, TUBA1B+CD8$^+$T_cells-C2, TUBA4A+CD8$^+$T_cells-C3, TUBB4B+CD8$^+$T_cells-C4, TUBA1A+Mac-C2, and DYNC1H1+Mac-C4 were all

downregulated in responders, indicating their potential role in ICB resistance among Bladder Urothelial Carcinoma (BLCA) patients (Figure S4H). Subsequently, we conducted Kaplan-Meier analysis in the TCGA, RECA-EU, E-MATB-1980, and IMvigor210 cohorts, pinpointing several novel aggrephagy cell clusters that significantly impacted Overall Survival (OS) in both ccRCC and population cohorts (Figures S3, S4, S5 and S6). Interestingly, analysis of all three ccRCC datasets revealed that four prognostic genes—TUBA1A, TUBA1B, TUBA4A, and HSP90AA1—were statistically significant across all datasets.

**3.7 Protein analysis of prognostic genes was performed.**

We systematically evaluated the protein expression levels of four key prognostic genes, TUBA1A, TUBA1B, TUBA4A, and HSP90AA1, using integrated bioinformatic and experimental approaches. Analysis of the CPTAC dataset via UALCAN revealed significantly reduced protein expression of TUBA1A, TUBA4A, and HSP90AA1 in ccRCC compared to normal tissues (Figure 8A). To validate these findings, we performed proteomic profiling of clinical ccRCC and paired normal tissues. Interestingly, this analysis showed significant upregulation of TUBA1B and TUBA4A in tumor samples (Figure 8B). Based on this consistent dysregulation across datasets, we selected TUBA4A for further experimental validation. We observed decreased protein expression levels of TUBA4A in ccRCC tissues compared to normal tissues (Figure 8C-8D). To further characterize TUBA4A, we examined its subcellular distribution using GeneCards, which indicated cytoplasmic and cytoskeletal localization, consistent with its potential role in cellular structural regulation. IHC results of the protein expression of TUBA4A from the HPA database were displayed in Figure 8E. We found that TUBA4A was expressed at a high level in normal tissues and exhibited various expression levels in ccRCC patients, ranging from low to high expression. Consistently, elevated TUBA4A protein levels were also observed in ccRCC cell lines (ACHN and Caki-1) compared to the 293T reference line (Figure 8F). In functional support of these findings, Kaplan–Meier analysis of TCGA-KIRC data further revealed that high FAP mRNA expression was significantly correlated with poorer overall survival in ccRCC patients (Figure 8G). Collectively, by integrating public database mining, proteomic profiling,

and experimental protein detection, we consistently identify aberrant TUBA4A expression in ccRCC, highlighting its potential role in tumor pathogenesis. The recurrent dysregulation of TUBA4A observed across these complementary analytical platforms implies the presence of context-specific regulatory mechanisms and solidifies its candidacy for in-depth functional and mechanistic exploration.

### 3.8 Oncogenic Behaviors Are Potentiated by TUBA4A via Autophagy Induction

To investigate the functional impact of TUBA4A, which is downregulated in ccRCC, we transfected ACHN and Caki-1 cells with a TUBA4A overexpression plasmid and confirmed elevated protein expression by Western Blot (Figure 9A). Functional assays revealed that TUBA4A overexpression significantly enhanced pro-liferation (MTS assay, Figure 9B), migration (Wound Healing and Transwell Migration assays), and invasion (Transwell Invasion assay) in both cell lines (Figure 9C-9D).

Given the association between TUBA4A and aggrephagy identified in our bioinformatic analyses, and considering that aggrephagy represents a critical subtype of selective autophagy [57], we examined classic autophagy markers. Overexpression of TUBA4A induced an elevation in the LC3-II/LC3-I ratio and accelerated degradation of P62, consistent with established hallmarks of autophagy induction [58]. As an α-tubulin isotype and a major component of cytoskeletal microtubules [27], TUBA4A may contribute to enhanced microtubule stability and function. Microtubules are known to support essential cellular processes including intracellular transport, organelle positioning, and cell motility [59], all of which are integral to autophagic flux. We propose that TUBA4A overexpression reinforces microtubule-mediated transport, thereby facilitating autophagosome formation and cargo degradation, as reflected by the accumulation of LC3 and reduction of P62 (Figure 9E). In summary, these results suggest that TUBA4A overexpression drives pro-tumorigenic phenotypes in ccRCC cells, potentially through the activation of autophagy. This proposed mechanism requires further functional validation.

## Discussion

Aggrephagy has recently emerged as a critical process in tumor biology, with its dysregulation strongly implicated in tumorigenesis and cancer progression [60, 61].

Although aggrephagy is considered a therapeutic target for proteinopathies, its cell-type-specific functions in the TME of ccRCC remain unexplored. In this study, we present the first single-cell atlas of aggrephagy activity in ccRCC, revealing heterogeneity across stromal and immune compartments and demonstrating that aggrephagy subtypes are closely associated with patient prognosis, thereby underscoring their clinical relevance.

Among stromal components, CAFs are key mediators of extracellular matrix remodeling and immunosuppression [62]. Distinct CAF subtypes have been described [63], with some shown to impair T-cell infiltration and limit PD-1 blockade efficacy [64]. Here, we identified two major CAF clusters: DYNC1I2+CAF-C1, enriched in metabolic signaling, pro-inflammatory pathways, and endothelial interactions, which correlated with favorable prognosis; and TUBB4B+CAF-C2, enriched in Ras/contractile signaling and pan-iCAF features, associated with poorer outcomes. Both subtypes showed differential transcription factor (TF) activity and enrichment in autophagy/aggrephagy-related pathways such as ER protein processing and phagosome formation [65, 66], suggesting that aggrephagy may shape CAF heterogeneity and influence immune suppression.

Macrophages are abundant in ccRCC and strongly linked to poor prognosis [67, 68]. Our analysis revealed that most aggrephagy-related TAM clusters exhibited M1-like signatures. Notably, TUBB4B+Mac-C0 displayed strong endothelial interactions and correlated with adverse prognosis, whereas HSP90AA1+Mac-C3 was transcriptionally active in ER protein processing and enriched for STAT1/STAT2/IRF1 activity. In contrast, TUBA1A+Mac-C2 was enriched in metabolic pathways, highlighting functional divergence among TAM aggrephagy subtypes [69, 70]. These findings suggest that aggrephagy modulates TAM metabolic and functional states, potentially contributing to immune evasion.

In adaptive immunity, $CD8^+$ T cells are central to antitumor defense [71, 72]. In ccRCC patients, these immune cells are involved not only in the anti-tumor response but also in cancer progression, with $CD8^+$ T cells playing a particularly significant role [73]. We found that TUBA1B+$CD8^+$T-C2 clusters exhibited enhanced communication

with endothelial cells, enrichment in metabolic and exhaustion pathways, and were associated with poor prognosis. TF analysis revealed distinct regulatory patterns across aggrephagy subtypes: CAF clusters showed activation of FOXC1, ATF4, and FOSB, whereas TUBA1B+CD8$^+$T-C2 clusters displayed broad TF inhibition, including STAT1 and ETS1, both implicated in cancer progression [74, 75].

Importantly, our study also highlights TUBA4A, a previously underexplored α-tubulin isoform, as a novel regulator within the ccRCC TME. TUBA4A is a major component of the cytoskeleton and plays essential roles in microtubule stability, intracellular transport, and cell motility [27]. We observed that TUBA4A expression correlates with aggrephagy-related signatures across multiple TME cell types, suggesting that its dysregulation may alter cytoskeletal dynamics, thereby affecting autophagic flux and immune–stromal interactions. Previous studies have shown that microtubule-associated proteins can regulate autophagosome trafficking and immune cell function [76, 77], supporting our finding that TUBA4A may serve as a structural and functional mediator linking cytoskeletal remodeling, aggrephagy activation, and TME reprogramming in ccRCC.

Collectively, our integrative single-cell analyses reveal that aggrephagy-related gene programs, including TUBA4A, shape the functional heterogeneity of CAFs, TAMs, and CD8$^+$ T cells, thereby influencing the immunosuppressive TME and patient prognosis in ccRCC. While limited by sample size, our study provides the first evidence that aggrephagy contributes to tumor–immune–stromal crosstalk in ccRCC, offering a novel perspective for therapeutic intervention. Future studies with larger cohorts are warranted to validate these findings and to explore aggrephagy and TUBA4A as potential targets for overcoming immune evasion.

## Conclusion

This study provides the first single-cell atlas of aggrephagy in the ccRCC TME, revealing its role in immune suppression, metabolic reprogramming, and therapeutic resistance. We identify TUBA4A as a novel autophagy-related oncogene that enhances

autophagic flux and promotes malignant phenotypes. These findings highlight aggrephagy and TUBA4A as potential biomarkers and therapeutic targets in ccRCC.

**Acknowledgments**

We acknowledge and appreciate our colleagues for their valuable efforts and comments on this paper.

**Abbreviations**

| | |
|---|---|
| ccRCC | clear cell renal cell carcinoma |
| RCC | renal cell carcinoma |
| TME | tumor microenvironment |
| NMF | non-negative matrix factorization |
| ICB | immune checkpoint blockade |
| TAMs | tumor-associated macrophages |
| scRNA-Seq | Single-cell RNA sequencing |
| CAFs | tumor-associated fibroblasts |
| TCGA | The Cancer Genome Atlas |
| ICGC | International Cancer Genome Consortium |
| RECA-EU | renal cell cancer cohort |
| OS | overall survival |
| TF | transcription factor |
| CPTAC | Clinical Proteomic Tumor Analysis Consortium |
| IHC | immunohistochemistry |

**Author Contributions**

QZ and KC were responsible for the entire experiment design. QD and KC did experimental validation with the help of WL, ZT, YD, ZB, YL, LY and YD. A bioinformatics assay was conducted by KC and ZX. The proteomic detection was analyzed by WL, ZT, XL, AS, JX, JZ and HS. KC and QD checked all results, organized figures, and wrote the manuscript with the help of QZ and ZY. All authors checked and approved the final version of this manuscript.

**Funding**

This work was supported by the National Natural Science Foundation of China (No. 82560591, 82460510, 82203565, 82103388, 31960145), Yunnan province applied research funds (202201AY070001-011, 202201AY070001-043, and 202301AS07001), the Science and Technology Innovation Team of Tumor Metabolism Research, Kunming Medical University (CXTD202102), and Scientific Research Fund of the Education Department of Yunnan Province (2025S004).

**Availability of data and materials**

All data generated or analyzed during this study are included in this published article.

**Data availability statement**

The data used to support the findings of this study are available from the corresponding author upon request.

**Declarations**

**Ethics approval and consent to participate**

Not Applicable.

**Consent for publication**

Not Applicable.

**Competing interests**

The authors declare that they have no conflicts of interests.

## References

1. Hsieh, J.J., et al., Renal cell carcinoma. Nat Rev Dis Primers, 2017. 3: p. 17009.
2. Padala, S.A., et al., Epidemiology of Renal Cell Carcinoma. World J Oncol, 2020. 11(3): p. 79-87.
3. Ricketts, C.J., et al., The Cancer Genome Atlas Comprehensive Molecular Characterization of Renal Cell Carcinoma. Cell Rep, 2018. 23(1): p. 313-326 e5.
4. Weaver, C., et al., Diagnostic and Prognostic Biomarkers in Renal Clear Cell Carcinoma. Biomedicines, 2022. 10(11).
5. Barata, P.C. and B.I. Rini, Treatment of renal cell carcinoma: Current status and future directions. CA Cancer J Clin, 2017. 67(6): p. 507-524.
6. Posadas, E.M., S. Limvorasak, and R.A. Figlin, Targeted therapies for renal cell carcinoma. Nat Rev Nephrol, 2017. 13(8): p. 496-511.
7. Takyar, S., et al., First-line therapy for treatment-naive patients with advanced/metastatic renal cell carcinoma: a systematic review of published randomized controlled trials. Anticancer Drugs, 2016. 27(5): p. 383-97.
8. Kamli, H., L. Li, and G.C. Gobe, Limitations to the Therapeutic Potential of Tyrosine Kinase Inhibitors and Alternative Therapies for Kidney Cancer. Ochsner J, 2019. 19(2): p. 138-151.
9. Linehan, W.M., Genetic basis of kidney cancer: role of genomics for the development of disease-based therapeutics. Genome Res, 2012. 22(11): p. 2089-100.
10. Makhov, P., et al., Resistance to Systemic Therapies in Clear Cell Renal Cell Carcinoma: Mechanisms and Management Strategies. Mol Cancer Ther, 2018. 17(7): p. 1355-1364.

11. Dagogo-Jack, I. and A.T. Shaw, Tumour heterogeneity and resistance to cancer therapies. Nat Rev Clin Oncol, 2018. 15(2): p. 81-94.
12. Gong, X., et al., Exosomes: A potential tool for immunotherapy of ovarian cancer. Front Immunol, 2022. 13: p. 1089410.
13. Xiong, J., et al., Revolutionizing anti-tumor therapy: unleashing the potential of B cell-derived exosomes. Front Immunol, 2023. 14: p. 1188760.
14. Zhao, Y., et al., IL-7: A promising adjuvant ensuring effective T cell responses and memory in combination with cancer vaccines? Front Immunol, 2022. 13: p. 1022808.
15. Lei, Y., et al., Applications of single-cell sequencing in cancer research: progress and perspectives. J Hematol Oncol, 2021. 14(1): p. 91.
16. Hwang, B., J.H. Lee, and D. Bang, Single-cell RNA sequencing technologies and bioinformatics pipelines. Exp Mol Med, 2018. 50(8): p. 1-14.
17. Papalexi, E. and R. Satija, Single-cell RNA sequencing to explore immune cell heterogeneity. Nat Rev Immunol, 2018. 18(1): p. 35-45.
18. Parzych, K.R. and D.J. Klionsky, An overview of autophagy: morphology, mechanism, and regulation. Antioxid Redox Signal, 2014. 20(3): p. 460-73.
19. Kocaturk, N.M., et al., Autophagy as a molecular target for cancer treatment. Eur J Pharm Sci, 2019. 134: p. 116-137.
20. Malampati, S., et al., Targeting Aggrephagy for the Treatment of Alzheimer's Disease. Cells, 2020. 9(2).
21. Miller, D.R. and A. Thorburn, Autophagy and organelle homeostasis in cancer. Dev Cell, 2021. 56(7): p. 906-918.
22. Ma, X., et al., CCT2 is an aggrephagy receptor for clearance of solid protein aggregates. Cell, 2022. 185(8): p. 1325-1345 e22.
23. Ano Bom, A.P., et al., Mutant p53 aggregates into prion-like amyloid oligomers and fibrils: implications for cancer. J Biol Chem, 2012. 287(33): p. 28152-62.
24. Kanapathipillai, M., Treating p53 Mutant Aggregation-Associated Cancer. Cancers (Basel), 2018. 10(6).
25. Silva, J.L., et al., Expanding the prion concept to cancer biology: dominant-negative effect of aggregates of mutant p53 tumour suppressor. Biosci Rep, 2013. 33(4).
26. Garcia-Mata, R., Y.S. Gao, and E. Sztul, Hassles with taking out the garbage: aggravating aggresomes. Traffic, 2002. 3(6): p. 388-96.
27. Breuss, M.W., et al., Tubulins and brain development - The origins of functional specification. Mol Cell Neurosci, 2017. 84: p. 58-67.
28. Su, C., et al., Single-Cell RNA Sequencing in Multiple Pathologic Types of Renal Cell Carcinoma Revealed Novel Potential Tumor-Specific Markers. Front Oncol, 2021. 11: p. 719564.
29. Davidson, G., et al., Mesenchymal-like Tumor Cells and Myofibroblastic Cancer-Associated Fibroblasts Are Associated with Progression and Immunotherapy Response of Clear Cell Renal Cell Carcinoma. Cancer Res, 2023. 83(17): p. 2952-2969.
30. Mariathasan, S., et al., TGFbeta attenuates tumour response to PD-L1 blockade by contributing to exclusion of T cells. Nature, 2018. 554(7693): p. 544-548.

31. Subramanian, A., et al., Gene set enrichment analysis: a knowledge-based approach for interpreting genome-wide expression profiles. Proc Natl Acad Sci U S A, 2005. 102(43): p. 15545-50.
32. Satija, R., et al., Spatial reconstruction of single-cell gene expression data. Nat Biotechnol, 2015. 33(5): p. 495-502.
33. Ohashi, N., et al., Plasma Soluble (Pro)renin Receptor Reflects Renal Damage. PLoS One, 2016. 11(5): p. e0156165.
34. Young, M.D., et al., Single-cell transcriptomes from human kidneys reveal the cellular identity of renal tumors. Science, 2018. 361(6402): p. 594-599.
35. Zhang, X., et al., CellMarker: a manually curated resource of cell markers in human and mouse. Nucleic Acids Res, 2019. 47(D1): p. D721-D728.
36. Chen, Y.P., et al., Single-cell transcriptomics reveals regulators underlying immune cell diversity and immune subtypes associated with prognosis in nasopharyngeal carcinoma. Cell Res, 2020. 30(11): p. 1024-1042.
37. Zhang, Y., et al., Glycogen metabolism-mediated intercellular communication in the tumor microenvironment influences liver cancer prognosis. Oncol Res, 2024. 32(3): p. 563-576.
38. Qiu, X., et al., Reversed graph embedding resolves complex single-cell trajectories. Nat Methods, 2017. 14(10): p. 979-982.
39. Vento-Tormo, R., et al., Single-cell reconstruction of the early maternal-fetal interface in humans. Nature, 2018. 563(7731): p. 347-353.
40. Guan, X., et al., Androgen receptor activity in T cells limits checkpoint blockade efficacy. Nature, 2022. 606(7915): p. 791-796.
41. Van de Sande, B., et al., A scalable SCENIC workflow for single-cell gene regulatory network analysis. Nat Protoc, 2020. 15(7): p. 2247-2276.
42. Wu, Y., et al., Spatiotemporal Immune Landscape of Colorectal Cancer Liver Metastasis at Single-Cell Level. Cancer Discov, 2022. 12(1): p. 134-153.
43. Hanzelmann, S., R. Castelo, and J. Guinney, GSVA: gene set variation analysis for microarray and RNA-seq data. BMC Bioinformatics, 2013. 14: p. 7.
44. Fu, J., et al., Large-scale public data reuse to model immunotherapy response and resistance. Genome Med, 2020. 12(1): p. 21.
45. Zhang, Q., et al., G6PD promotes renal cell carcinoma proliferation through positive feedback regulation of p-STAT3. Oncotarget, 2017. 8(65): p. 109043-109060.
46. Chandrashekar, D.S., et al., UALCAN: A Portal for Facilitating Tumor Subgroup Gene Expression and Survival Analyses. Neoplasia, 2017. 19(8): p. 649-658.
47. Edwards, N.J., et al., The CPTAC Data Portal: A Resource for Cancer Proteomics Research. J Proteome Res, 2015. 14(6): p. 2707-13.
48. Uhlen, M., et al., Proteomics. Tissue-based map of the human proteome. Science, 2015. 347(6220): p. 1260419.
49. Li, C., et al., Cancer-associated associated-fibroblast-derived exosomes in cancer progression. Mol Cancer, 2021. 20(1): p. 154.
50. Zhu, Y., et al., Metabolic reprogramming and crosstalk of cancer-related fibroblasts and immune cells in the tumor microenvironment. Front Endocrinol (Lausanne), 2022. 13: p. 988295.
51. Affo, S., et al., Promotion of cholangiocarcinoma growth by diverse cancer-associated fibroblast subpopulations. Cancer Cell, 2021. 39(6): p. 883.

52. Sun, X., et al., Single-cell dissection reveals the role of aggrephagy patterns in tumor microenvironment components aiding predicting prognosis and immunotherapy on lung adenocarcinoma. Aging (Albany NY), 2023. 15(23): p. 14333-14371.

53. Liberzon, A., et al., The Molecular Signatures Database (MSigDB) hallmark gene set collection. Cell Syst, 2015. 1(6): p. 417-425.

54. Kovaleva, O.V., et al., Tumor Associated Macrophages in Kidney Cancer. Anal Cell Pathol (Amst), 2016. 2016: p. 9307549.

55. Cui, C., et al., Neoantigen-driven B cell and CD4 T follicular helper cell collaboration promotes anti-tumor CD8 T cell responses. Cell, 2021. 184(25): p. 6101-6118 e13.

56. Pandey, P., et al., Review to Understand the Crosstalk between Immunotherapy and Tumor Metabolism. Molecules, 2023. 28(2).

57. Lamark, T. and T. Johansen, Aggrephagy: selective disposal of protein aggregates by macroautophagy. Int J Cell Biol, 2012. 2012: p. 736905.

58. Klionsky, D.J., et al., Guidelines for the use and interpretation of assays for monitoring autophagy (4th edition)(1). Autophagy, 2021. 17(1): p. 1-382.

59. Brouhard, G.J. and L.M. Rice, Microtubule dynamics: an interplay of biochemistry and mechanics. Nat Rev Mol Cell Biol, 2018. 19(7): p. 451-463.

60. Marsh, T. and J. Debnath, Autophagy suppresses breast cancer metastasis by degrading NBR1. Autophagy, 2020. 16(6): p. 1164-1165.

61. Poillet-Perez, L. and E. White, Role of tumor and host autophagy in cancer metabolism. Genes Dev, 2019. 33(11-12): p. 610-619.

62. Mao, X., et al., Crosstalk between cancer-associated fibroblasts and immune cells in the tumor microenvironment: new findings and future perspectives. Mol Cancer, 2021. 20(1): p. 131.

63. Galbo, P.M., Jr., X. Zang, and D. Zheng, Molecular Features of Cancer-associated Fibroblast Subtypes and their Implication on Cancer Pathogenesis, Prognosis, and Immunotherapy Resistance. Clin Cancer Res, 2021. 27(9): p. 2636-2647.

64. Li, L., et al., Laminin gamma2-mediating T cell exclusion attenuates response to anti-PD-1 therapy. Sci Adv, 2021. 7(6).

65. Morishita, H. and N. Mizushima, Diverse Cellular Roles of Autophagy. Annu Rev Cell Dev Biol, 2019. 35: p. 453-475.

66. Nakatogawa, H., Mechanisms governing autophagosome biogenesis. Nat Rev Mol Cell Biol, 2020. 21(8): p. 439-458.

67. Dong, K., et al., FCER1G positively relates to macrophage infiltration in clear cell renal cell carcinoma and contributes to unfavorable prognosis by regulating tumor immunity. BMC Cancer, 2022. 22(1): p. 140.

68. Xu, W., et al., Tumor-associated macrophage-derived chemokine CCL5 facilitates the progression and immunosuppressive tumor microenvironment of clear cell renal cell carcinoma. Int J Biol Sci, 2022. 18(13): p. 4884-4900.

69. Mehla, K. and P.K. Singh, Metabolic Regulation of Macrophage Polarization in Cancer. Trends Cancer, 2019. 5(12): p. 822-834.

70. Wang, S., et al., Metabolic Reprogramming Induces Macrophage Polarization in the Tumor Microenvironment. Front Immunol, 2022. 13: p. 840029.

71. Krishna, C., et al., Single-cell sequencing links multiregional immune landscapes and tissue-resident T cells in ccRCC to tumor topology and therapy efficacy. Cancer Cell, 2021. 39(5): p. 662-677 e6.

72. Monjaras-Avila, C.U., et al., The Tumor Immune Microenvironment in Clear Cell Renal Cell Carcinoma. Int J Mol Sci, 2023. 24(9).

73. Matsuki, M., et al., Tumor-infiltrating CD8(+) T cells recognize a heterogeneously expressed functional neoantigen in clear cell renal cell carcinoma. Cancer Immunol Immunother, 2022. 71(4): p. 905-918.

74. Nguyen, C.T.K., et al., AIRE is induced in oral squamous cell carcinoma and promotes cancer gene expression. PLoS One, 2020. 15(2): p. e0222689.

75. Chen, M., et al., Emerging roles of activating transcription factor (ATF) family members in tumourigenesis and immunity: Implications in cancer immunotherapy. Genes Dis, 2022. 9(4): p. 981-999.

76. Kast, D.J. and R. Dominguez, The Cytoskeleton-Autophagy Connection. Curr Biol, 2017. 27(8): p. R318-R326.

77. Bento, C.F., et al., Mammalian Autophagy: How Does It Work? Annu Rev Biochem, 2016. 85: p. 685-713.

# Figures

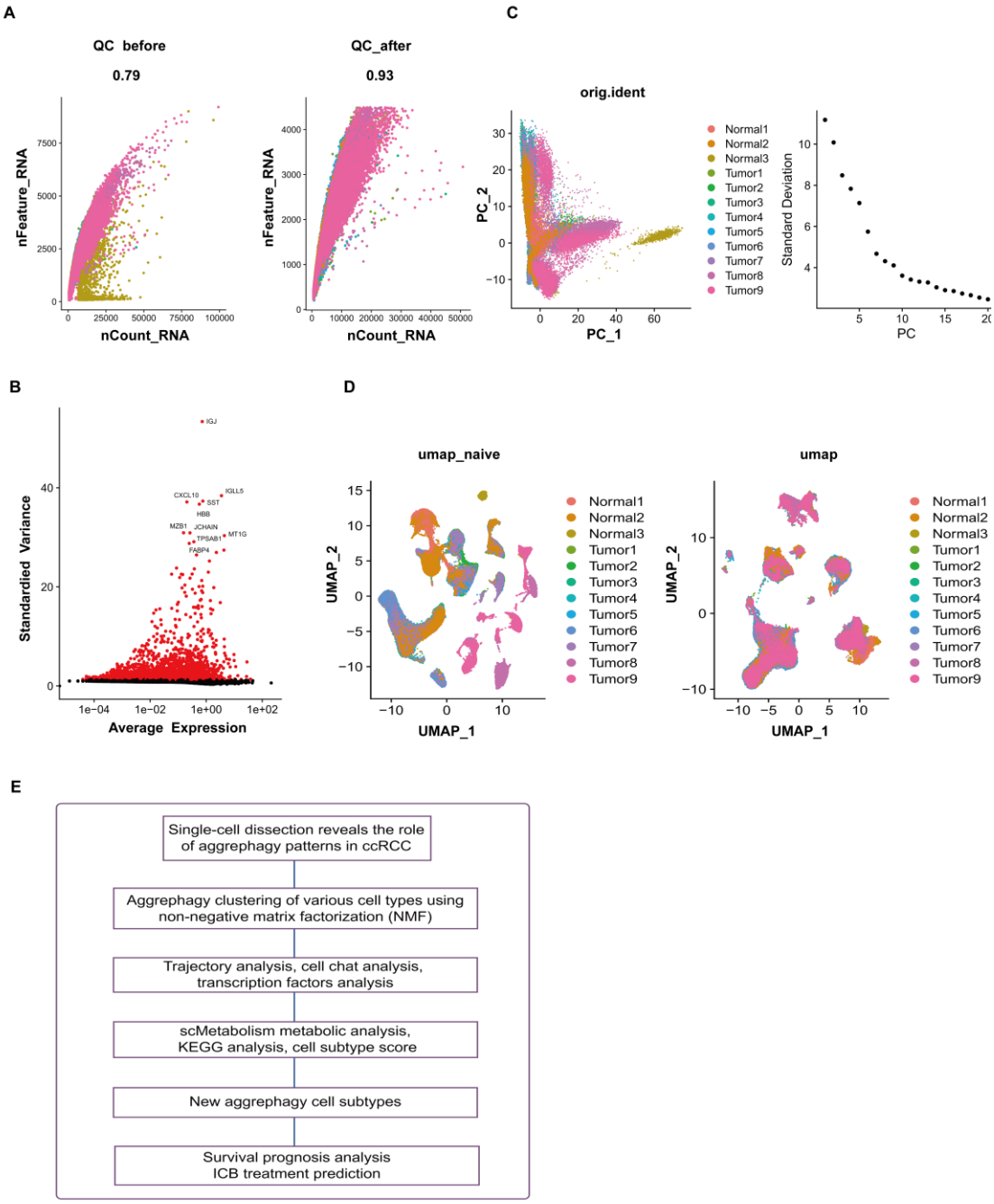


**Figure 1. The single-cell quality control process and overall design were presented. (A)** The cells were uniformly distributed in the ccRCC samples, and a positive association (r = 0.93) was observed between gene expression levels and the amount of gene expression. **(B)** Ten hypervariable genes were identified. **(C)** The highly variable genes were normalized and visualized using DimPlot and ElbowPlot. **(D)** The distribution of tumors and normal tissues before (umap_naive) and after (umap) harmony was shown by UMAP. **(E)** The overall design of this study was illustrated.

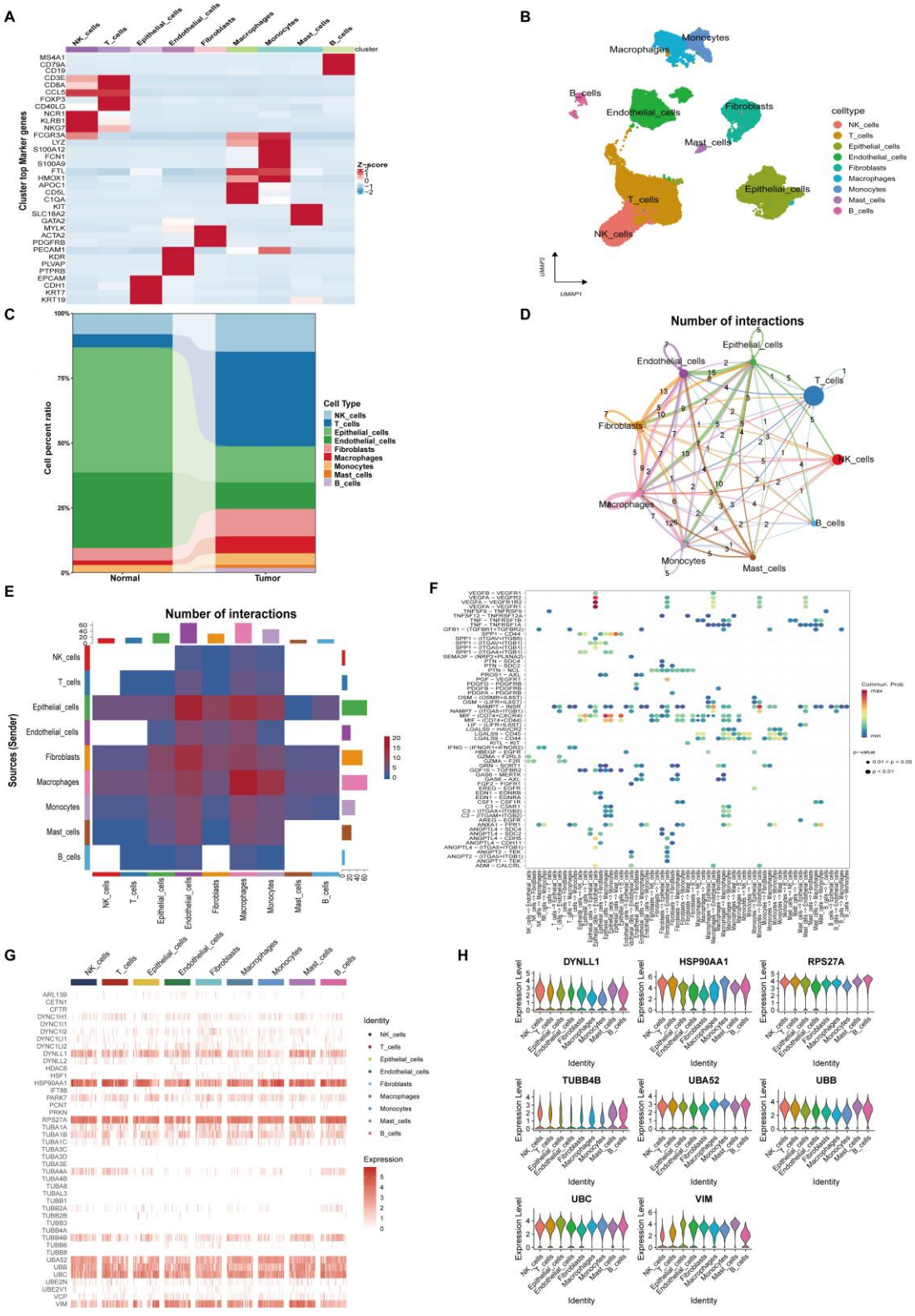


**Figure 2. An overview of aggrephagy-related genes in single-cell data from ccRCC is provided. (A)** Subpopulations of ccRCC cells are annotated with marker genes in a heat map. **(B)** Nine distinct cell subpopulations within ccRCC cells are identified using UMAP visualization. **(C)** The proportion of cell subpopulations in both normal and ccRCC tissues is demonstrated in a cell

percentage diagram. **(D-E)** Cellular interactions among subpopulations of ccRCC cells are revealed using CellChat analysis. **(F)** Interaction levels through ligand-receptor pairs among ccRCC cell subtypes are depicted in a ligand-receptor dot plot. **(G)** The distribution of aggrephagy-related genes in NK cells, T cells, epithelial cells, endothelial cells, fibroblasts, macrophages, monocytes, mast cells, and B cells is exhibited by a heat map. **(H)** The expression of aggrephagy-related genes in TME subpopulation cells is illustrated in violin diagrams.

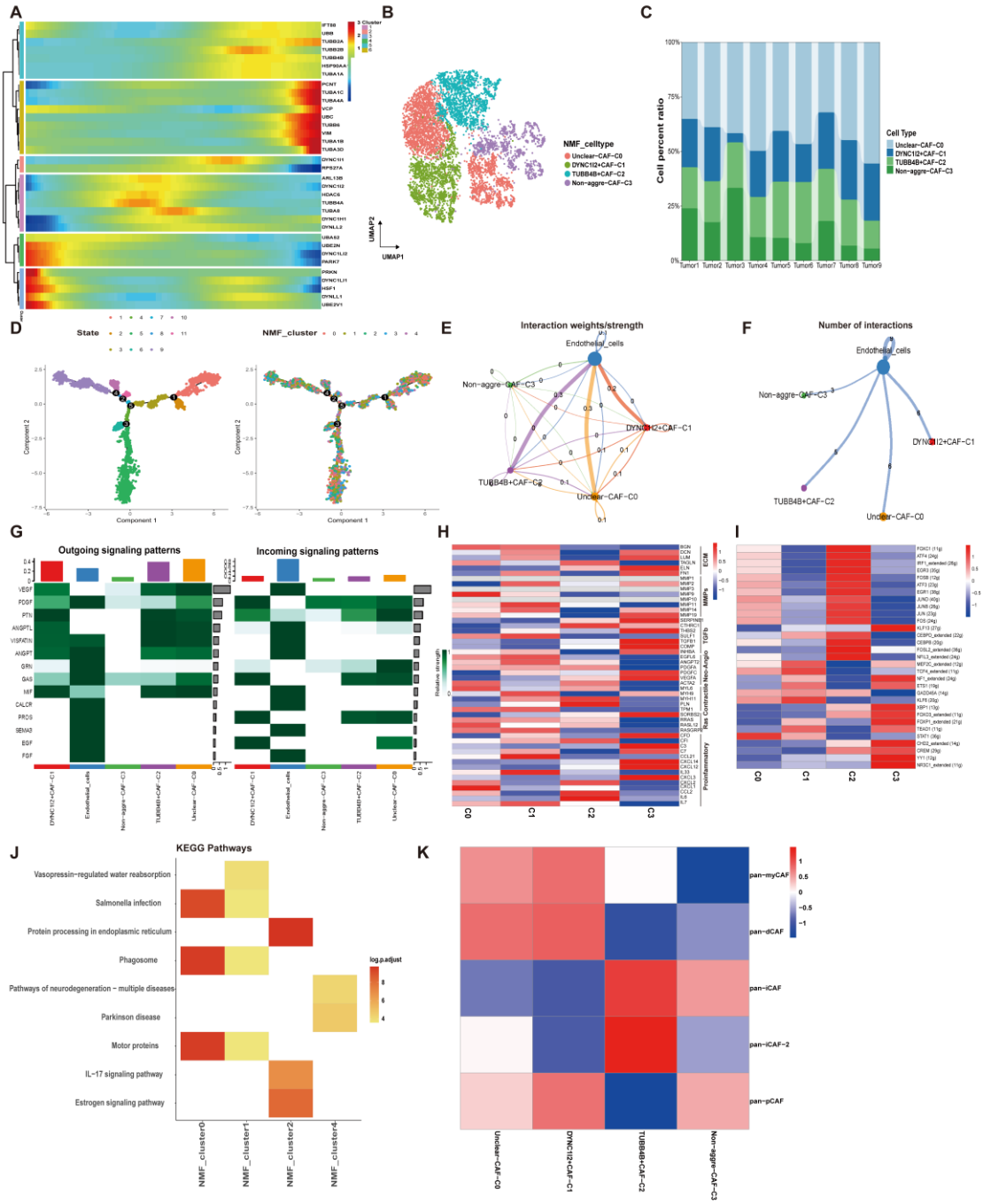


**Figure 3. Novel fibroblast clusters are evaluated under aggrephagy gene modifications. (A)** The differentiation of fibroblast clusters after NMF classification is exhibited by pseudo-time analysis. **(B)** Fibroblast clusters after aggrephagy gene annotation are displayed using UMAP. **(C)** The proportion of novel fibroblast clusters in nine ccRCC patients is shown by a cell percentage diagram. **(D)** The role of aggrephagy genes in fibroblast clustering after NMF classification is revealed through trajectory analysis. **(E-F)** The interaction of novel fibroblast clusters with endothelial cells is revealed through CellChat analysis. **(G)** The signaling pathways of the novel

fibroblast cluster inputs and outputs are illustrated in a heat map. **(H)** The expression of CAF phenotype markers in novel fibroblast clusters is shown in a heat map. **(I)** The active expression of transcription factors in a novel cell cluster of aggrephagy fibroblasts is depicted by a heat map. **(J)** KEGG enrichment analysis of the aggrephagy fibroblast cluster enrichment is conducted. **(K)** The enrichment of aggrephagy fibroblast clusters in a characteristic subpopulation of previous fibroblasts is demonstrated by a heat map.

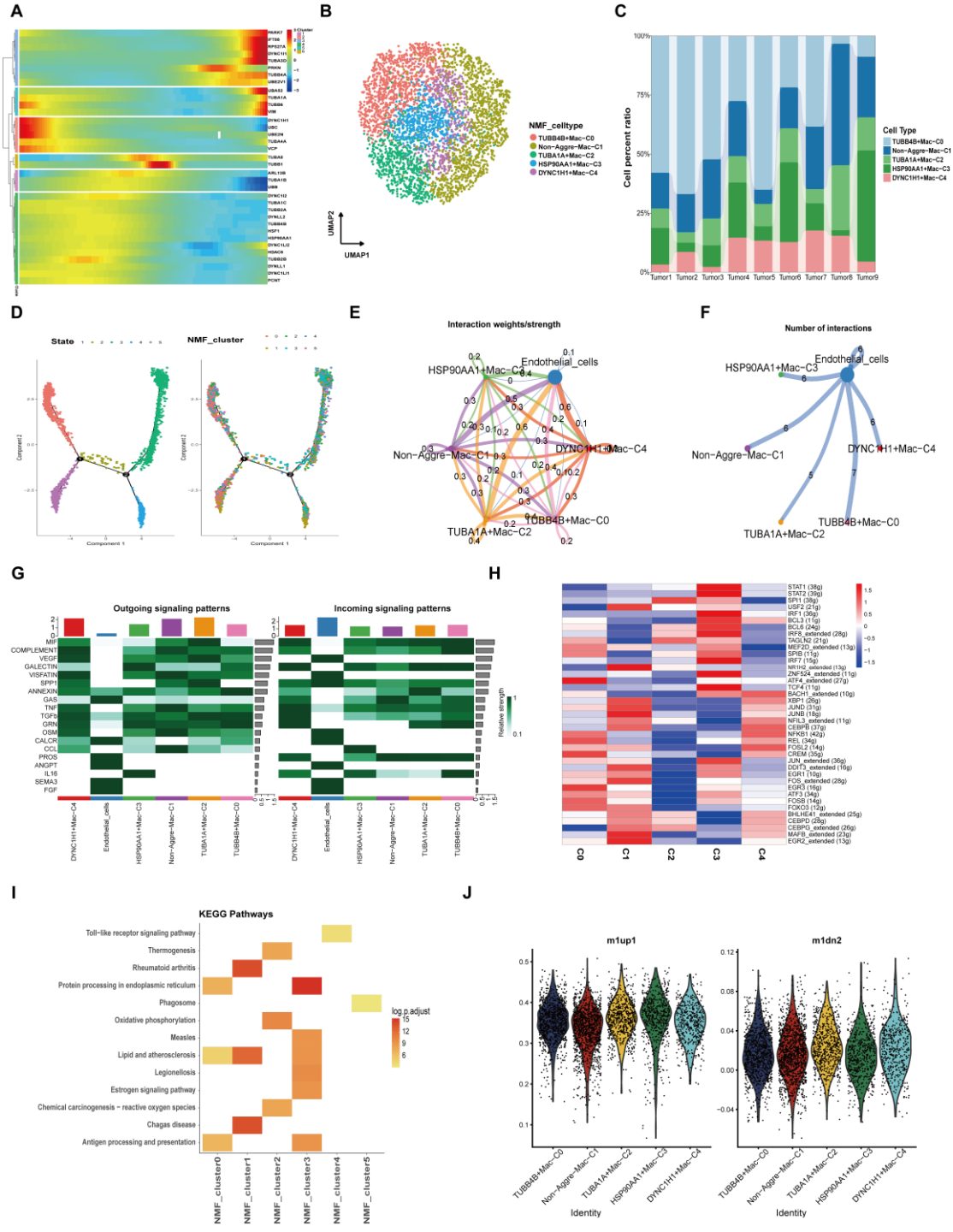


**Figure 4. Novel macrophage cell clusters are studied under aggrephagy gene modifications.**

**(A)** Differentiation of macrophages after NMF classification is demonstrated by pseudo-time analysis. **(B)** Novel aggrephagy macrophage clusters after clustering by NMF are shown in UMAP. **(C)** The expression of novel aggrephagy macrophage cell clusters in patients with ccRCC is depicted in cell percentage plots. **(D)** The role of aggrephagy genes in macrophage clustering after

NMF classification is revealed by trajectory analysis. **(E-F)** The interaction of novel macrophage cell clusters with endothelial cells is revealed by CellChat. **(G)** The signaling pathways of the novel macrophage cell cluster inputs and outputs are displayed in a heat map. **(H)** Transcription factor activities of aggrephagy macrophage cell clusters are illustrated in a heat map. **(I)** KEGG enrichment analysis is performed for macrophage cell clusters enrichment. **(J)** The expression of novel aggrephagy macrophage clusters in M1 and M2 phenotypes is shown in a violin diagram.

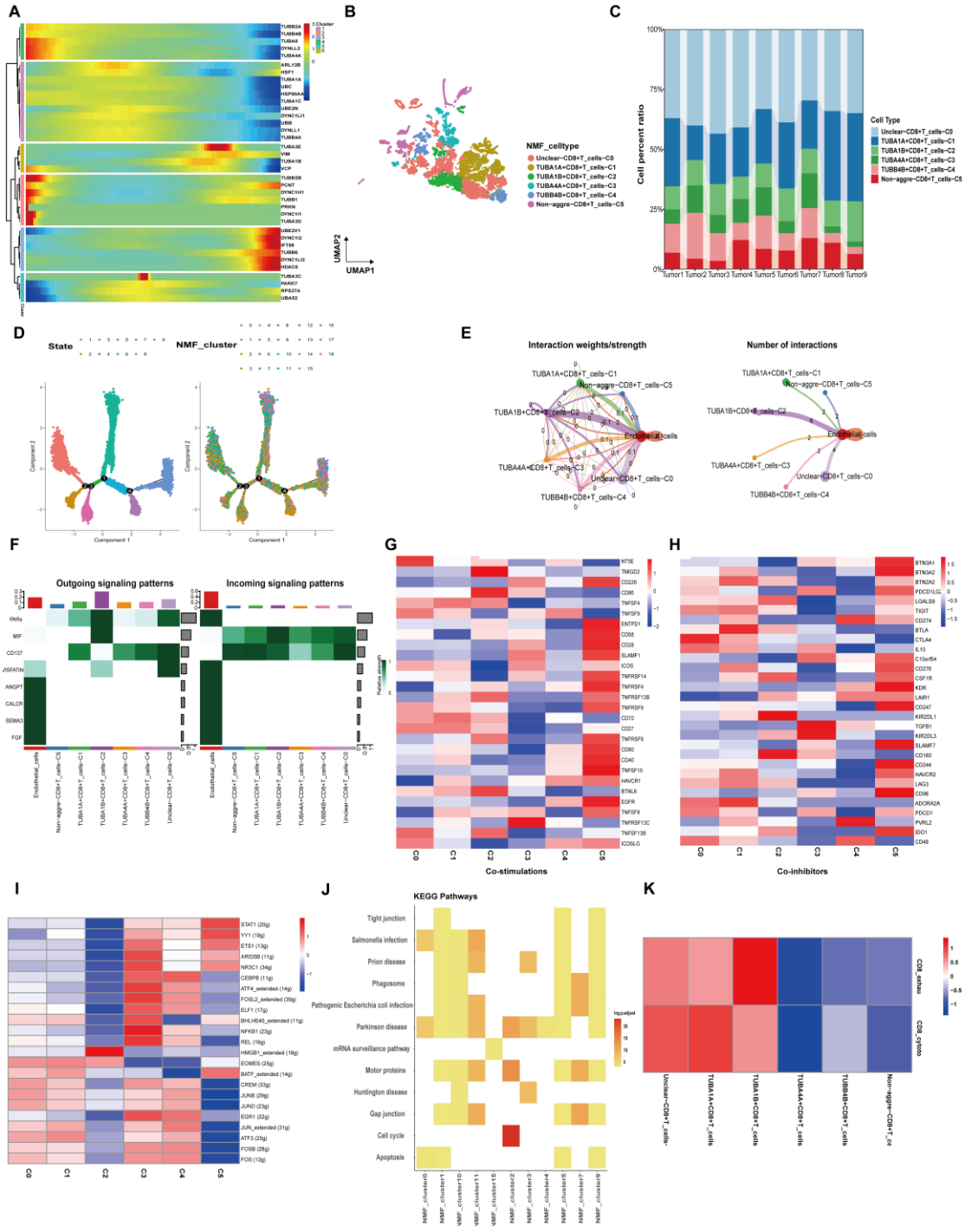


**Figure 5. Novel CD8$^+$ T cell clusters are analyzed under aggrephagy gene modifications. (A)** Differentiation of CD8$^+$ T cell clusters after NMF classification is demonstrated by pseudo-time analysis. **(B)** CD8$^+$ T cell clustering fractionation after aggrephagy annotation is illustrated using UMAP. **(C)** The percentage of expression of novel aggrephagy CD8$^+$ T cell clusters is showcased by cell percentage plots. **(D)** The role of aggrephagy genes in CD8$^+$ T cell clustering after NMF classification is presented by trajectory analysis. **(E)** The interaction of novel CD8$^+$ T cell clusters

with endothelial cells is demonstrated by Cell Chat. **(F)** The signaling pathways of the novel $CD8^+$ T cell clusters' inputs and outputs are depicted by a heat map. **(G)** Expression of immunostimulatory genes in novel $CD8^+$ T cell clusters is shown in a heat map. **(H)** Expression of immunoinhibitory genes in novel $CD8^+$ T cell clusters is displayed in a heat map. **(I)** Transcription factor activities of aggrephagy $CD8^+$ T cell clusters are revealed in a heat map. **(J)** Enrichment of metabolic signaling pathways in aggrephagy $CD8^+$ T cell clusters is presented in a dot plot. **(K)** KEGG enrichment analysis is performed for the enrichment of aggrephagy $CD8^+$ T cell clusters. **(L)** The correlation of novel aggrephagy $CD8^+$ T cell subtype cells with $CD8^+$ T cells exhaustion and cytotoxicity is manifested by a heat map.

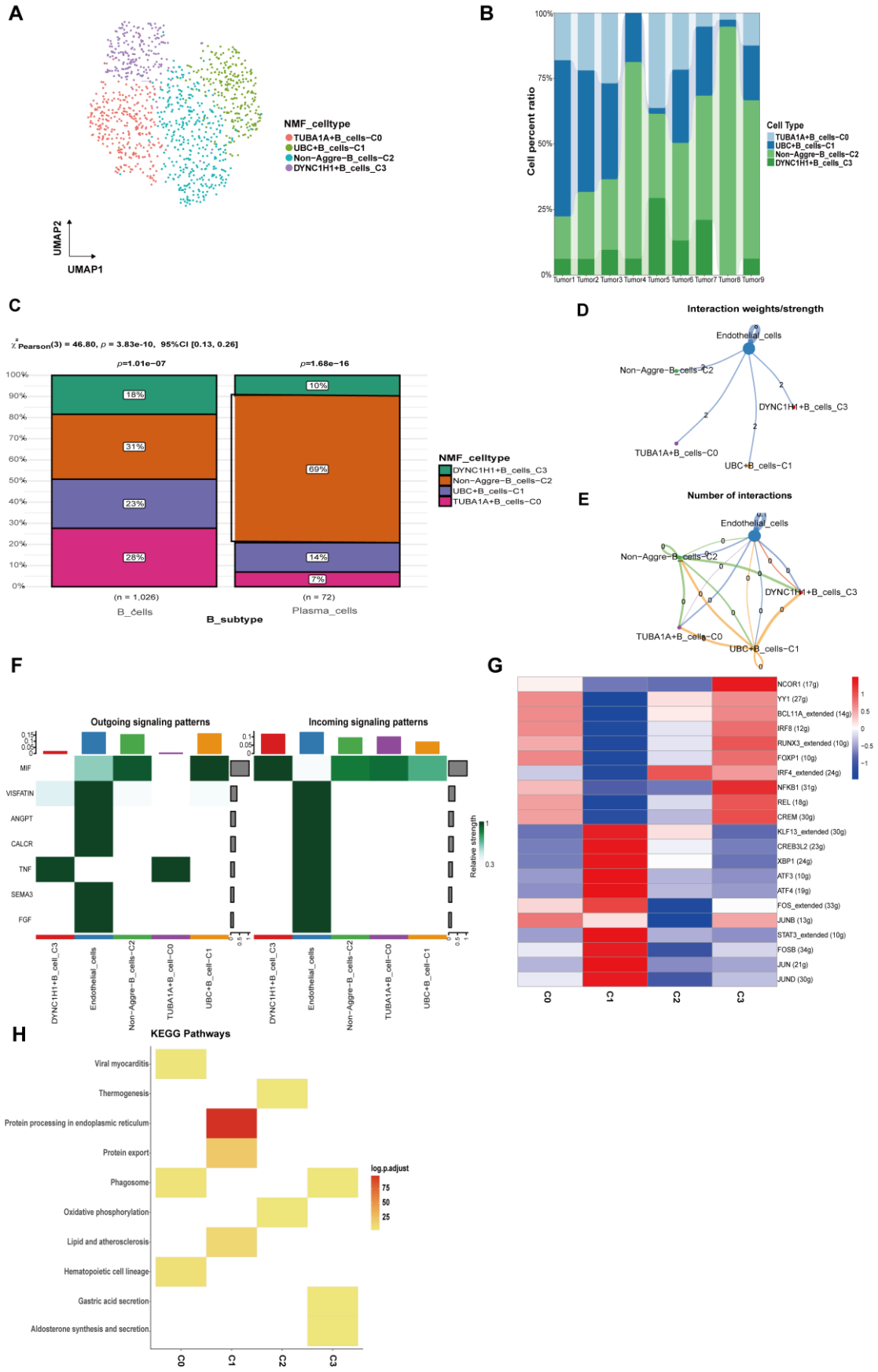


**Figure 6. Novel B cell clusters are investigated under aggrephagy gene modifications. (A)** B cell clustering fractionation after aggrephagy annotation is demonstrated by UMAP. **(B)** The

percentage of expression of novel aggrephagy B cell clusters in nine ccRCC patients is shown in a cell percentage diagram. **(C)** The expression of novel aggrephagy B cell clusters and plasma cells in patients with ccRCC is shown in cell percentage plots. **(D-E)** The interaction of novel B cell clusters with endothelial cells is illustrated by Cell Chat. **(F)** The signaling pathways of the novel B cell clusters' inputs and outputs are manifested in a heat map. **(G)** Transcription factor activities of aggrephagy B cell clusters are demonstrated in a heat map. **(H)** The enrichment of metabolic signaling pathways in aggrephagy B cell clusters is depicted in a dot plot. **(I)** KEGG enrichment analysis is performed for the aggrephagy B cell clusters enrichment.

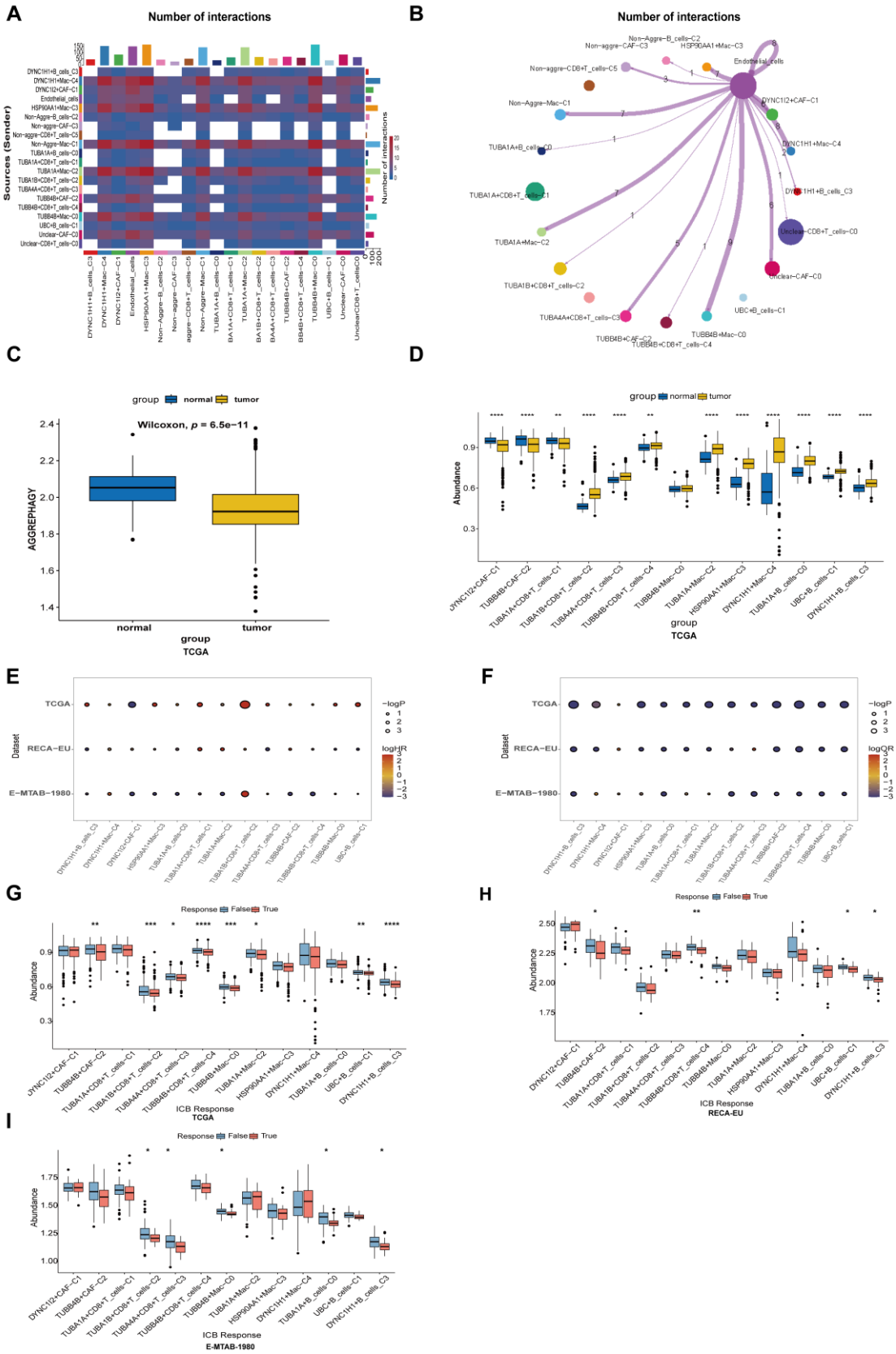


**Figure 7. The prognosis and immune response of patients with ccRCC are influenced by novel aggrephagy cell clusters. (A)** Interactions between all novel aggrephagy cell clusters are

demonstrated by Cell Chat. **(B)** The interaction between all novel aggrephagy cell clusters and endothelial cells is demonstrated by Cell Chat. **(C)** The difference in aggrephagy gene expression in ccRCC tissues and normal tissues is shown in a box plot. **(D)** The difference in expression of aggrephagy cell clusters in ccRCC tissues and normal tissues is demonstrated in a box plot. **(E)** One-way Cox analysis of novel aggrephagy cell clusters in the prognosis of TCGA, RECA-EU and E-MTAB-1980 patient cohorts is shown in a bubble plot. **(F)** One-way Cox analysis of novel aggrephagy cell clusters in the immune response prognosis of TCGA, RECA-EU and E-MTAB-1980 patient cohorts is demonstrated in a bubble plot. **(G-I)** The immune response of aggrephagy cell clusters in TCGA, RECA-EU and E-MTAB-1980 patient cohorts is shown in box plots. $*p < 0.05$, $**p < 0.05 < 0.01$, $***p < 0.05 < 0.001$, $****p < 0.05 < 0.0001$.

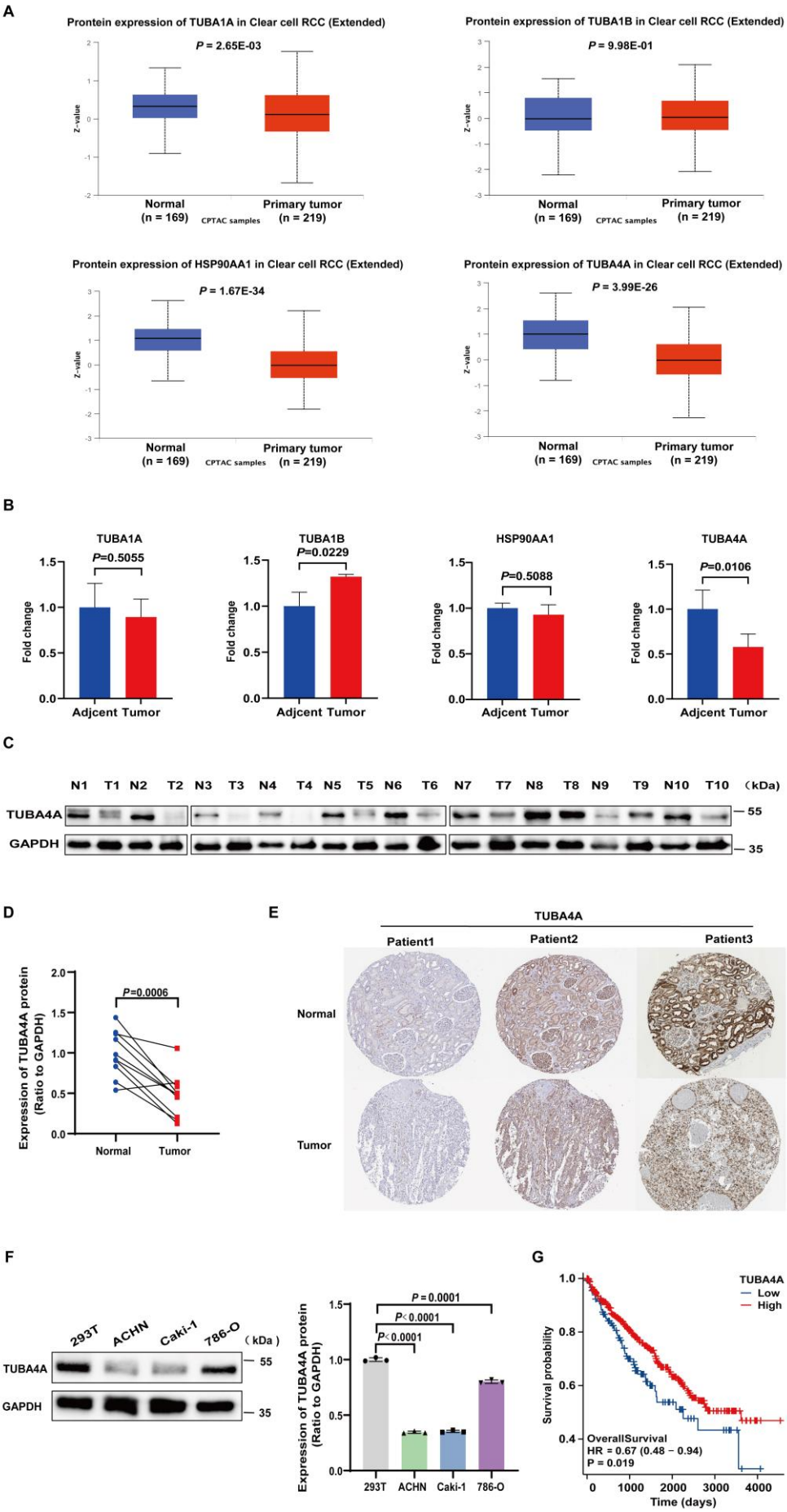

**Figure 8. Protein analysis of prognostic genes was performed. (A)** The protein expression levels of TUBA1A, TUBA1B, TUBA4A and HSP90AA1 were assessed based on data from CPTAC. **(B)** Proteomic analysis was conducted to confirm the four prognostic genes in ccRCC specimens and adjacent normal tissues (n=20). **(C-E)** The protein expression levels of TUBA4A in paired normal tissues and ccRCC samples (n=10, C-D) were detected by Western blot analysis and the relevant data were obtained from the HPA online database (E). **(F)** The protein expression of TUBA4A was detected in normal renal tubular epithelial cells (293T) and ccRCC cell lines (ACHN, Caki-1 and 786-O) using Western blot analysis. **(G)** The overall survival (OS) curves were constructed based on TCGA data (low = 134, high = 407). Note: $*p < 0.05$, $**p < 0.01$, $***p < 0.001$, ns, nonsignificant vs. each control.

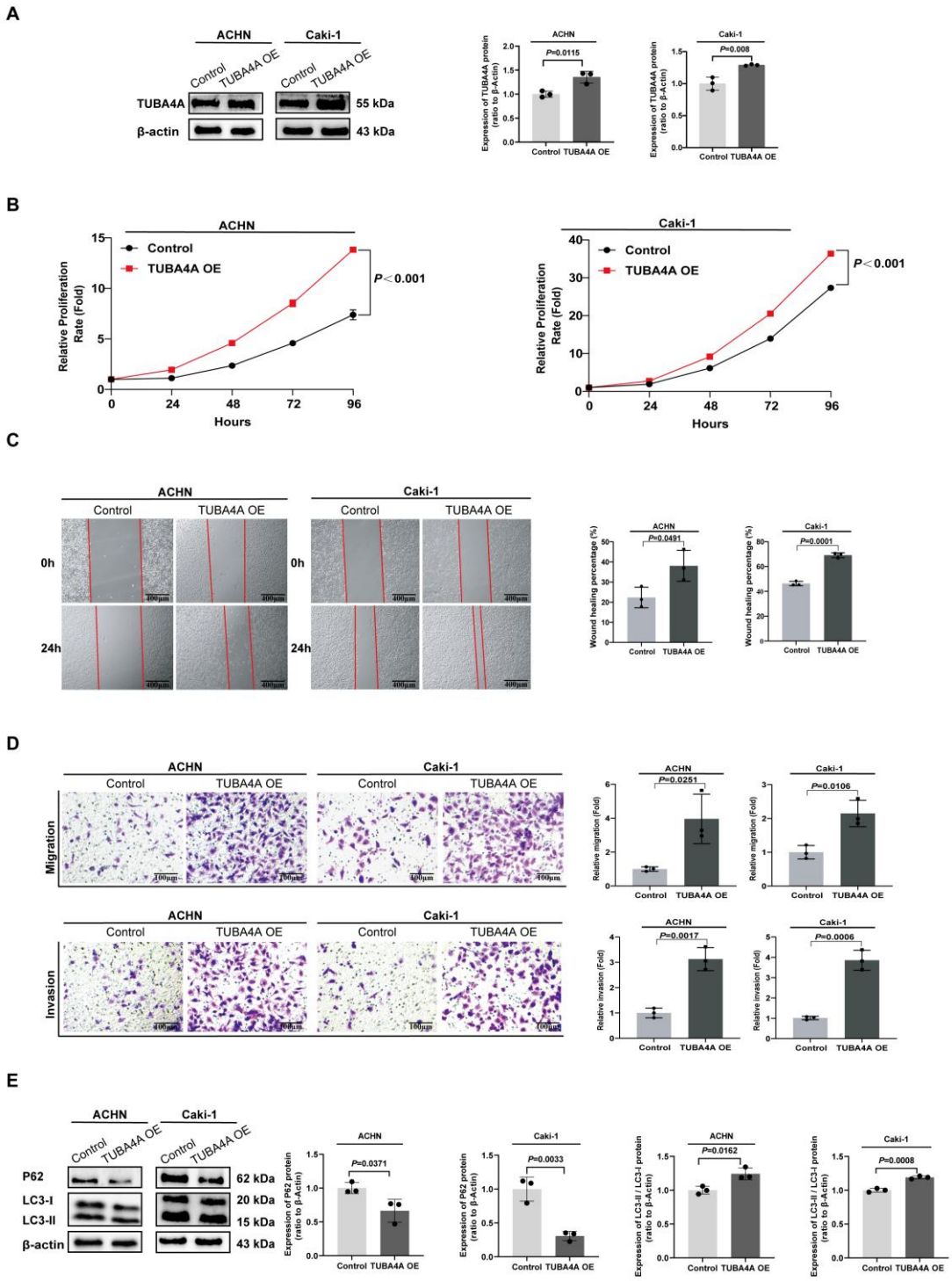


**Figure 9. ccRCC cells' proliferation was promoted by TUBA4A overexpression in vitro. (A, E)** TUBA4A (A), LC3 and P62 (E) expression was detected in ccRCC cell lines after transfection with the TUBA4A overexpression plasmid through Western Blot analysis. **(B-D)** MTS assay (B), Scratch assay (C), Transwell migration assay and Transwell invasion assay (D) were used to detect the effect of TUBA4A overexpression on cell proliferation, migration, and invasion in ccRCC cell

lines. Bars represent the mean ± SD from three independent experiments, each performed in triplicate. *$p < 0.05$, **$p < 0.01$, ***$p < 0.001$, ns, nonsignificant vs. each control. OE, overexpression.